



**HAL**  
open science

## The wave regimes of the Central Pacific Ocean with a focus on pearl farming atolls

Cyril Dutheil, Swen Jullien, Jérôme Aucan, Christophe E. Menkès, Romain Le Gendre, Serge Andréfouët

► **To cite this version:**

Cyril Dutheil, Swen Jullien, Jérôme Aucan, Christophe E. Menkès, Romain Le Gendre, et al.. The wave regimes of the Central Pacific Ocean with a focus on pearl farming atolls. *Marine Pollution Bulletin*, 2021, 162, pp.111751. 10.1016/j.marpolbul.2020.111751 . hal-03195787

**HAL Id: hal-03195787**

**<https://hal.science/hal-03195787v1>**

Submitted on 13 Feb 2023

**HAL** is a multi-disciplinary open access archive for the deposit and dissemination of scientific research documents, whether they are published or not. The documents may come from teaching and research institutions in France or abroad, or from public or private research centers.

L'archive ouverte pluridisciplinaire **HAL**, est destinée au dépôt et à la diffusion de documents scientifiques de niveau recherche, publiés ou non, émanant des établissements d'enseignement et de recherche français ou étrangers, des laboratoires publics ou privés.



Distributed under a Creative Commons Attribution - NonCommercial 4.0 International License

1           **The wave regimes of the Central Pacific Ocean with a focus on pearl farming atolls**

2

3           **Cyril Dutheil<sup>1,2,3</sup>, S. Jullien<sup>4</sup>, J. Aucan<sup>1</sup>, C. Menkes<sup>1</sup>, R. Le Gendre<sup>5</sup>, S. Andréfouët<sup>1</sup>**

4

5   <sup>1</sup> Institut de Recherche pour le Développement, UMR 9220 ENTROPIE (Institut de Recherche Pour  
6 le Développement, Université de la Réunion, Université de Nouvelle-Calédonie, Ifremer, Centre  
7 National de la Recherche Scientifique), BP A5, 98848 Nouméa cedex, New-Caledonia

8   <sup>2</sup> IRD, LOCEAN (UMR 7159), BP A5, 98848 Nouméa cedex, New-Caledonia

9   <sup>3</sup>Department of Physical Oceanography and Instrumentation, Leibniz Institute for Baltic Sea  
10 Research Warnemünde, Rostock, Germany.

11   <sup>4</sup> Ifremer, Univ. Brest, CNRS, IRD, Laboratoire d'Océanographie Physique et Spatiale (LOPS),  
12 IUEM, Plouzané, France

13   <sup>5</sup> IFREMER, ENTROPIE (UMR 9220), Institut de Recherche pour le Développement, Université de  
14 la Réunion, Université de Nouvelle-Calédonie, Centre National de la Recherche Scientifique, BP  
15 32078, 98897 Noumea Cedex, New-Caledonia

16

17 Corresponding author: Cyril Dutheil ([cyril.dutheil@io-warnemuende.de](mailto:cyril.dutheil@io-warnemuende.de))

## 18 **Abstract**

19 Pearl farming sustainability in South Central Pacific (SCP) atolls strongly depends on water quality  
20 and renewal. These factors are partly controlled by the wave conditions that impact the lagoon  
21 circulation. To characterize the wave conditions around 83 SCP atolls including those hosting pearl  
22 farming activities, we used 18 years of WaveWatchIII simulation with a grid refined from 50 to 5km  
23 resolution. Three regional wave regimes are statistically identified: two associated with long distant  
24 swells originating from mid-latitude storms, and one with local trade winds. All regimes occur with  
25 a relatively high frequency (22-44%), but with a marked seasonality. Wave conditions are also  
26 strongly modified locally during their propagation between the archipelagoes. Western and southern  
27 isolated atolls generally have a single regime all around their rims. In contrast, central Tuamotu  
28 atolls experience different regimes depending on their levels of protection. These results help  
29 understanding atoll hydrodynamics, which has implications for their management.

30 **Key-words:** Wave regimes; atoll hydrodynamics; atoll rim; Tuamotu; Cook Islands, WaveWatchIII

31

## 32 **1. Introduction**

33 Atolls are a type of coral reef formation characterized by an inside lagoon separated from  
34 the ocean by an atoll rim, which can be partly opened with passes and shallow spillways (called  
35 *hoa* in Polynesian, Woodroffe and .Biribo, 2011) that allow the intermittent exchange of seawater  
36 between the lagoon and the ocean. The world largest atoll-only archipelago is the Tuamotu-Gambier  
37 chain, located in French Polynesia, with 77 atolls, including 72 with lagoons (not dried or uplifted;  
38 Andréfouët and Adjeroud, 2019). Several atolls and lagoons are also present in the Society  
39 Archipelago and further west in the Cook Islands. Understanding the physical and biological  
40 functioning of their lagoons is capital for local population because marine life often provides  
41 directly or indirectly their main resources with coastal fisheries, tourism, and for many locations,  
42 black pearl farming. The latter activity is the 2<sup>nd</sup> source of income of French Polynesia, and a major  
43 activity in nearly half of the South Central Pacific (SCP) atolls.

44 The black pearl farming activities, namely spat collection and rearing, and their  
45 sustainability are highly dependent on water renewal and quality (Rodier et al., 2019). In addition to  
46 tide, atoll lagoon water renewal and circulation are mainly controlled by wind and wave conditions  
47 (Andréfouët et al., 2001a, 2006; Callaghan et al., 2006). Several studies have shown that wind  
48 directly influences lagoon circulation via its surface stress, while waves breaking over the reef have  
49 an indirect influence on lagoon circulation by initiating water transport from the open ocean to the

50 lagoon through the rim (Atkinson et al., 1981; Kraines et al., 1999; Tartinville et al., 1997). These  
51 transfers depend on the geomorphology of the atoll (rim elevation, degree of aperture) but also on  
52 incident wave conditions (height, period, direction) (Andréfouët et al., 2001a; Caldwell and Aucan,  
53 2007; Callaghan et al., 2006; Dumas et al., 2012; Hoeke et al., 2013; Tartinville and Rancher, 2000).  
54 However, little is known on the long-term wave regimes experienced by each atoll, and influencing  
55 their water quality and pearl farming potential.

56 Further investigations are thus warranted to enhance the characterization of the wave  
57 regimes in the SCP region, around and close to each individual atoll. Early work in the late 1990s  
58 (Young, 1999) gathered along-track altimetry data and compiled atlases. Then, Tartinville and  
59 Rancher (2000), followed by Andréfouët et al. (2001), looked at the relationship between altimetry  
60 data and flow through the atoll rims to infer the turnover time of atoll lagoons. Andréfouët et al.  
61 (2012), using 11 years of model and altimetry data, showed that events responsible for high wave  
62 height around the Tuamotu archipelago are either associated with southern swells, strong easterly  
63 winds, western local storms, or distant tropical cyclone passage, with the southern atolls of the  
64 archipelago experiencing more frequently large swells (higher than 2.5m) than the western Tuamotu  
65 atolls. Andréfouët et al., (2012) also showed that the incident waves conditions in the Tuamotu  
66 archipelago can drastically change from one atoll to another due to the shadowing effect generated  
67 by the these atolls (Chawla and Tolman, 2008; Delpy et al., 2010). Finally, Andréfouët et al. (2015)  
68 explained the occurrences of lagoon mass mortality events in the region by a combination of  
69 significant wave height, temperature and wind conditions. To go further, and understand if and how  
70 different atolls have different potential for pearl farming on the long term, it is necessary to  
71 characterize the wave climate in the region and for each individual atoll.

72 The present study depicts the wave regimes at multiple spatial scales around atolls, from  
73 the regional SCP scale to the atoll rim scale, by using a simulation with a multigrid approach, which  
74 allows such a downscaling. A statistical study based on k-means and hierarchical classifications is  
75 performed to robustly characterize the wave conditions, accounting not only for the wave height but  
76 also for the wave period and direction. The large-scale origin, the frequency of occurrence and the  
77 seasonal variability of regional wave regimes are computed. Along with wind regimes depicted by  
78 Dutheil et al. (2020), these results bring a new understanding of the environment of pearl farming  
79 atolls.

80

## 81 **2. Materials and Methods**

## 82 2.1 Study area

83 The study area is the South Central Pacific (SCP) region (130°W–165°W and 9°S–25°S;  
84 Fig. 1a, smaller box in Fig. 1b,c). The atoll scale analysis focuses on 80 sites from Tuamotu,  
85 Gambier and Society archipelagoes (all in French Polynesia), and 3 from Cook Islands. Studied  
86 sites include atolls with a central water body (true lagoon, not dry or uplifted) and two high islands  
87 (Aitutaki and Mangareva), which have been called pseudo-atolls considering their wide lagoons.  
88 For simplicity, all 83 sites will be hereafter referred as atolls. The atolls exhibit a large range of  
89 degree of closure (or aperture) to the ocean. From west to east, the density of atolls also varies  
90 significantly. The highest density of atolls, and the largest ones, are found in the central western  
91 Tuamotu (Fig. 1). Conversely, Cook Islands, East Tuamotu, and Gambier atolls are much more  
92 isolated. The most equatorial site is Manihiki in Cook Islands, the most austral sites are Mangareva  
93 and Temoe. The largest atoll in the domain is Rangiroa (1446 km<sup>2</sup>) while the smallest studied atolls  
94 cover less than a couple of kilometer square.

95

## 96 2.2 Data and Modeling

### 97 • 2.2.1 Model configuration

98 The wave model used in the present study is the WAVEWATCH III (hereafter WW3;  
99 Tolman, 2009) spectral model version 6.07 (<https://polar.ncep.noaa.gov/waves/wavewatch/>). The  
100 model configuration consists of a multigrid approach with 2 two-way nested domains: a global  
101 domain at 0.5° resolution in which a first two-way nesting is performed at 0.25°, that encompasses  
102 the tropical South Pacific region (162°E-126°W; 5°N-30°S, black box in Fig. 1), and a second two-  
103 way nesting at 0.05° resolution around the atolls of interest (Fig. 1a). All grids are rectangular  
104 regular grids. The computation in the finer grid is only performed on delimited points around atolls  
105 (thanks to a masking procedure on the rectangular grid, see Fig. 1a) to limit computational cost. The  
106 open ocean points of our domain of interest masked in the 0.05° grid are thus computed on the  
107 0.25° grid. Model bathymetry is built by interpolating at the different grid resolutions the GEBCO  
108 30'' bathymetry (2014 version:  
109 [http://www.gebco.net/data\\_and\\_products/gridded\\_bathymetry\\_data/](http://www.gebco.net/data_and_products/gridded_bathymetry_data/)). In a region like French  
110 Polynesia where there is a large number of small islands and atolls, the blocking of ocean waves by  
111 these structures, too small to be resolved by a numerical grid, can be a major source of error in  
112 wave prediction models. This is why the use of an obstruction scheme is essential in this region.  
113 The obstruction scheme used here is that of Tolman (2003) which has been automated in Chawla et

114 Tolman (2008). From a very high resolution coastline, this scheme considers the proportion of the  
115 cell that is obscured in both x and y directions. These transparency parameters are then used as a  
116 coefficient to calculate the attenuation of the energy flow through the obscured cell. The spectral  
117 discretization (common to the 3 grids) is performed on 24 directions ( $15^\circ$ ), and 32 frequencies  
118 (from 0.0373 to 0.7159Hz with an increment factor of 1.1). The three model domains use the wave  
119 generation and dissipation parameterizations proposed by Ardhuin et al. (2010), and a third order  
120 propagation scheme (Tolman et al., 2002). Numerical schemes and parameterizations used in this  
121 configuration are summarized in Table 1. In particular, our simulations use the ST4 source term  
122 package from Ardhuin et al. (2010) with a wind-wave growth parameter,  $\beta_{\max}$ , adjusted to 1.6, and  
123 infra-gravity waves are parameterized following Ardhuin et al. (2014). Reflection at the coast is  
124 accounted for with a coefficient of 0.1 and with a dependence to frequency.

125 The 10-m wind forcing field is based on the European Centre for Medium-Range Weather  
126 Forecasts fifth generation atmospheric reanalysis of the global climate, ERA5 (DOI:  
127 10.24381/cds.adbb2d47) at  $0.25^\circ$  and hourly frequency. To better represent the effects of tropical  
128 cyclones, which are underestimated in this forcing, we replaced the ERA5 surface wind along  
129 tropical cyclone tracks by a statistical structure reconstructed from the observed maximum speed,  
130 retrieved in the best-tracks archive (<ftp://texmex.mit.edu/pub/emanuel/HURR/tracks/>). This  
131 methodology of forcing follows that of Vincent et al. (2012) and is fully detailed in Jullien et al. (*in*  
132 *prep.*). The ERA5 10-m wind field remains untouched out of cyclone tracks. The hindcast period for  
133 the present study covers the 2000-2017 period. January 2000 has been removed from the analysis  
134 because it is used for the spin-up period.

#### 135 • 2.2.2 Data and methods for WW3 validation

136 The Climate Change Initiative (CCI) sea state satellite dataset (Dodet et al., 2020; Piollé et  
137 al., 2020, <http://cci.esa.int/seastate>) is used for validation of the modelled significant wave height  
138 ( $H_s$ ). This dataset provides inter-calibrated and noise-corrected (Quilfen and Chapron, 2019)  
139 estimations of  $H_s$  from all available altimeter measurements over the period of interest. Coastal  
140 values in a 50km along-shore area flagged out because of the poor reliability of the data due to  
141 coastline interference with the signal. In order to perform an accurate comparison, the WW3 outputs  
142 are extracted along each satellite track and averaged over  $0.5^\circ$  grid cells to compute simulated vs  
143 observed significant wave height biases (Fig. 2).

144

### 145 2.3 Clustering methods

146 To identify wave regimes in the studied region, a statistical classification method is used to  
147 determine the main modes of wave variability during the 2000-2017 period. To that end, the daily  
148 average of the peak direction ( $D_p$ ), the peak frequency ( $F_p$ ) and the significant wave height ( $H_s$ ) are  
149 extracted from the 18-year WW3 simulation, which amounts to 6544 days. From  $D_p$ ,  $F_p$ , and  $H_s$ ,  
150 three parameters are computed  $\{H_s(t)*\cos(D_p(t)), H_s(t)*\sin(D_p(t)), 1/F_p(t)\}$ , following Lecacheux  
151 et al. (2012). At each grid point, the variables are centered and reduced by subtracting the temporal  
152 mean of the whole domain and by dividing by its standard deviation. The classification by wave  
153 regimes is then performed for three different spatial scales: regional, atolls, and atoll rim sections.

154 At the regional scale, the  $0.25^\circ$  grid is used and a principal component analysis (PCA;  
155 Jolliffe, 2011) is first performed on the 6544 days of the 3 parameters  $\{H_s(t)*\cos(D_p(t)),$   
156  $H_s(t)*\sin(D_p(t)), 1/F_p(t)\}$ , each day being treated as an individual vector for the PCA to extract the  
157 main modes of spatial variability. The first twenty principal components are kept, representing 80%  
158 of the cumulative total variance. In that reduced space, the 6544 days are classified using a k-means  
159 classification (Diday, 1971) to determine wave regimes. This approach allows identifying wave  
160 recurrent conditions at the regional scale. One of the limitations of k-means clustering algorithms is  
161 that they require defining *a priori* the number of clusters ( $k$ ), and many methods have been  
162 developed to determine the optimal number of clusters. The 'NbClust' function in factoextra R  
163 package allows comparing 26 of these methods (Charrad et al., 2014). The number of clusters kept  
164 corresponds to the most frequent between these 26 methods.

165 At the atoll scale, the finest  $0.05^\circ$  grid is used, and we define 8 geographical points (one by  
166 direction: North, North-East, East, South-East, South, Southwest, West, and Northwest) around  
167 each of the 83 atolls to extract our variables  $\{H_s(t)*\cos(D_p(t)), H_s(t)*\sin(D_p(t)), 1/F_p(t)\}$ . These  
168 points are manually pre-selected at around 8 kilometers of the atoll rim in each of the main  
169 directions (N, NE, E, SE, S, SW, W, NW), thus defining 8 domains. The exact position of these  
170 points depends also on the orientation of the atoll rim for each of these particular octants since most  
171 atolls have complex irregular shapes, and not circular shapes. Then the closest WW3 grid point is  
172 associated to the pre-defined points. For each atoll, the 3 parameters of the 8 surrounding points are  
173 concatenated and considered like one individual in the following. Then, a hierarchical classification  
174 algorithm (Euclidean distance and complete aggregation, using the 'Cluster' package in the R  
175 programming environment) is performed on these new 83 individuals. This approach identifies  
176 clusters of atolls that are characterized by a given wave climate around their entire periphery.

177 At the scale of the atoll rim geographical sectors, the same previous 8 points by atoll are  
178 considered but here each point is considered as an individual. The hierarchical classification is

179 performed for the 664 (83\*8) individual rim sections. This approach determines clusters of atoll  
180 rims characterized by a similar wave climate.

181

## 182 **2.4 Large scale wave origins**

183 We determine the geographical origins of the waves impacting our zone of interest by  
184 using the global wave model grid (Fig. 1b). In the open ocean, waves propagate along long circle  
185 routes or orthodromy. For each model grid point, we calculate the azimuth relative to the central  
186 point of our domain of interest (17.5°S, 144°W). Then for each grid point, the number of time steps  
187 for which the wave peak direction ( $D_p$ ) is within +/- 5 degree of the target azimuth is counted. A  
188 percentage of occurrence over the entire model period (2000-2017) is then computed seasonally,  
189 and year-round. Grid points where the occurrence is lower than 2% are discarded. This simple  
190 method allows to easily visualize the areas of wave generation that will ultimately impact the  
191 targeted region. Specific work for each atoll can be conducted, but here we considered the entire  
192 region, hence the computations are made only for its center. This method does not take into account  
193 the effects of refraction, reflection or blockage by small islands.

194

## 195 **3. Results**

### 196 **3.1 WW3 validation**

197 Figure 2 displays the difference of significant wave height ( $H_s$ ) between our WW3  
198 simulation and the altimetry measurements over the 2000-2017 period. Over the global domain  
199 (Fig. 2a), WW3 simulation tends to overestimate  $H_s$  by 20 to 30 cm in the Austral Ocean and areas  
200 impacted by tropical cyclones probably because of the wind vortex interpolation on the coarse  $\frac{1}{2}^\circ$   
201 induces a too wide fetch for these strong and localized events. It also underestimates  $H_s$  by 10 to 20  
202 cm in the semi-closed seas and regions dotted with islands possibly associated to the  
203 parameterization of sub-grid scale obstructions which may be too simple. This includes the SCP  
204 region although SCP is characterized by a low bias overall ( $\sim -5$ cm with few locations up to -20 or  
205 +5 cm). We also note that the bias in SCP is reduced by the higher model resolution around the  
206 atolls (not shown). Overall, these biases are relatively low and in the range of state-of-the-art wave  
207 models (Chawla et al., 2013; Rascle and Ardhuin, 2013).

208

### 209 **3.2 Regional wave regimes**



210 Three regional wave regimes was the consensus suggested by NbClust as the optimal  
211 number of clusters for the k-means algorithm. Figure 3 represents the temporal average of each  
212 cluster indices for the three variables (Hs, Dp, Tp=1/Fp).

213

### 214 **3.2.1 Characteristics of the regional wave regimes**

215 Regime 1 (R1) is a southwesterly incoming swell with a relatively high amplitude of 3.2m  
216 and a period of 14s (Fig. 3adg). The islands and atolls of the area, in particular the Tuamotu  
217 Archipelago, act as a natural barrier to this swell, strongly decreasing Hs down to 1.6m behind the  
218 denser part of the archipelago and 2.2m on the sides. The strong shadowing effect of the  
219 archipelago has the effect of rotating the mean waves direction anticlockwise and also affects the  
220 period of the swell which decreases to 13s and even less than 10 s behind the densest atoll area.

221 Regime 2 (R2) is characterized by south-south-east waves of 2.4m and 11.5s period (Fig.  
222 3beh). As for Regime 1, waves are impacted when crossing the archipelago with rotation in peak  
223 direction (from 170° to 120°N) and a decrease in height and period (down to Hs<1.8m, Tp<10s)  
224 north and west of the Tuamotu.

225 Finally, Regime 3 (R3) is a northwesterly swell in the northern part of grid domain with a  
226 lower incoming amplitude of Hs=2.0m, and a relatively long period of more than 13s (Fig. 3cfi). In  
227 the southern part of the domain, waves come from the south-southwest (~200°N) and have a  
228 slightly shorter period (Tp<=13s) and slightly higher Hs (Hs=2.2m) than in the northern part. In this  
229 regime, the shadowing effect of the archipelago is slightly different, with a less pronounced effect  
230 on the period, which decreases from 13.5s to 12.5-13s, an anticlockwise rotation of the waves from  
231 north-west to south-west direction, and a wave height which appears relatively low all around the  
232 archipelago (Hs=1.8m). Here, the Tuamotu Archipelago has a more widespread impact on the wave  
233 height compared to its much localized effect in R1. The mean incoming direction of the waves in  
234 R1 is indeed normal to the archipelago, while in R2 the waves cross the archipelago with an angle  
235 closer to its main orientation explaining the weaker but more widespread shadowing effect. This is  
236 also associated to the two incoming wave directions: north-west in the northern part and south-  
237 south-west in the southern part of the domain.

238 The three regimes have different frequencies of occurrence (from 22 to 44% of the time,  
239 Table 2) with R2 being the most frequent (44.7%) following by R3 (33.3%), and R1 (22%). Their  
240 seasonal occurrence (Fig. 4) reveals that the south-southeasterly regime (R2) occur all year long but  
241 with a higher frequency in austral autumn and winter. The southwesterly and northwesterly regimes  
242 (R1 and R3) have a very strong seasonality: R1 is almost absent during austral summer, and is

243 particularly frequent in austral winter, while R3 has an opposite behavior. This seasonality results  
244 from the wave origins.

245

### 246 **3.2.2 Large scale wave origins**

247 The waves impacting the SCP have different origins (Fig. 5). Incoming swells with longer  
248 periods (R1 and R3) are remotely-generated waves which originate from the mid-to-high latitudes  
249 of the northern and southern hemispheres (Fig. 5). These waves are generated by storms and  
250 therefore have a seasonal modulation, with higher occurrences during their respective winter season  
251 (Fig. 5b,c). Southern hemisphere waves impact our region all year long as shown in Fig. 4. The  
252 Austral Ocean region experiences strong winds and waves all year long, but with a stronger power  
253 in austral autumn-winter as highlighted by longer period and higher Hs in the southern part of the  
254 domain in R1 than in R3 (Fig. 3). Comparatively, northern hemisphere mid-latitude storms only  
255 occur in boreal winter (Fig. 5), and corresponding in R3 (Fig. 4) to the waves in the northern part of  
256 grid domain (Fig. 4). A third source of waves impacting our region is associated to the trade winds.  
257 These waves appear in R2 and have a seasonal distribution corresponding to the trade wind regime  
258 (see Dutheil et al. 2020). They are characterized by a shorter period associated to their more local  
259 origin. Let's note that as trade winds blow over the entire Pacific region, part of these waves can be  
260 locally generated, and part of them originate further east as shown in Fig. 5c.

261

### 262 **3.3 Wave regimes at atoll scale**

263 The previous section has pictured the regional pattern of wave regimes in the SCP,  
264 confirming that atolls generate or are subjected to a strong shadowing effect with very different  
265 wave conditions north and south of the Tuamotu archipelago, as well as in its different areas  
266 depending on the density, orientation, and size of atolls. Consequently, broad generalization is not  
267 granted and it appears mandatory to compute wave regimes at the atoll scale to properly assess the  
268 incoming wave conditions for each pearl farming atoll of interest.

269 Applying a hierarchical classification for the 83 atolls, we build the dendrogram  
270 represented in Figure 6. First, we consider 3 groups (C1, C2, C3) based on one similarity threshold,  
271 as indicated by the vertical black dashed line in Figure 6. Figure 7 shows the geographical position  
272 of the individuals of these 3 groups (green, red, and blue colors), and Table 3 their average wave  
273 characteristics. Clusters C1 and C2 have quite similar average characteristics, but the dendrogram  
274 separates these two clusters revealing that the average conditions mix different exposures to waves.

275 Indeed, the first cluster C1 (green) is located in the western part of the region and includes the Cook  
276 and the Society Islands (Fig. 7), and is characterized by strong exposure to northwestern and  
277 southwestern swells (R1 and R3 in Fig. 3). Cluster C2 (red, Fig. 7) groups the southeastern part of  
278 the Tuamotu atolls and the Gambier Archipelago. This cluster is more protected from the  
279 northwestern swells (R3) but exposed to the southern swells and trade winds (R1 and R2; Fig. 3).  
280 Finally, cluster C3 (blue) gathers the northern Tuamotu atolls, and appears as the less exposed  
281 cluster (mean wave height and period of 1.42m and 11.53s, Table 3). This area is indeed strongly  
282 protected for all regional regimes (see Fig. 3). It is however submitted to northwestern swells (R3 in  
283 Fig. 3) and trade winds, the latter appearing as the peak wave system for this area (Table 3, peak  
284 direction of 113.72).

285 The clustering structure is investigated at a second level for a lower similarity threshold  
286 that defines 13 clusters (dashed color boxes in Fig. 6). Interestingly, this new separation appears to  
287 follow very precisely the geographic limits of archipelagos and the north-south and east-west  
288 orientations for the Tuamotu Archipelago. The average characteristics of these 13 new clusters are  
289 summarized in Table 4. Cluster C1 is now divided into 3 clusters, distinguishing (Fig. 7) the  
290 northern Cook Islands (D3, green triangles), the southern Cook Islands (D2, green dot), and the  
291 Society Islands (D1, green squares). These 3 clusters slightly differ by their average conditions,  
292 notably with southern Cook Islands submitted to higher average waves but with a slightly lower  
293 period, and Society Islands showing waves with a more western peak direction than Cook Islands.  
294 This can be explained by the fact that Society Islands are exposed to less fetch during trade wind  
295 conditions, due to the protection by the Tuamotu Archipelago. Cluster C2 is split into 5 clusters  
296 separating the Gambier Archipelago (D8, red dots) showing the most energetic average wave  
297 conditions ( $H_s=2.05\text{m}$  and  $T_p=12.84\text{s}$ , Table 4) from the southern Tuamotu (D7, red squares),  
298 south-eastern Tuamotu (D4, red-crosses), and 2 clusters in the central Tuamotu (D6 red crosses, and  
299 D5 red triangles) with lower wave conditions ( $H_s=1.41\text{-}1.44$ , Table 3). All these clusters have an  
300 average south-south-west peak wave direction. Finally, cluster C3 is separated in 5 new clusters  
301 which show quite different wave conditions (Table 3). The most western cluster (D13, blue squares)  
302 is the less protected from long-incoming swell ( $T_p=12.19\text{s}$ ), but acts as a strong barrier, so that  
303 cluster D10 (blue circles), west to D13, features low wave conditions ( $H_s=1.27\text{m}$ ,  $T_p=10.52$ ), and a  
304 north-east average peak direction. Central and most north-eastern Tuamotu (D12, D11, D10, blue  
305 square-crosses, triangle, and crosses) are relatively protected and show an average peak directions  
306 varying from south-east to east. This clustering shows an important diversity of wave conditions,

307 especially in the central Tuamotu region depending on the atoll main exposure and on the  
308 shadowing effect by other atolls.

309

### 310 **3.4 Wave regimes at the scale of atoll rim sections**

311 It can be expected that rim sections with different orientations may be differently affected  
312 by waves with distinct directions and origins. To confirm this hypothesis, we finally perform a  
313 clustering on atoll rim sections (see section 2.3). The spatial distribution of the first five clusters of  
314 the dendrogram (not shown) are plotted in Figure 8.

315 The first cluster S1 (purple dots in Fig. 8) includes atolls from Cook Islands and Society. It  
316 occurs all around the atolls (Fig. 8abc). The second cluster S2 (green dots) gathers the rims and  
317 atolls in the south part of the study area, while S3 (blue dots) occurs in the north exposed rim  
318 sections of the Tuamotu, Society and Gambier archipelagos. Cluster S4 (red dots) and cluster S5  
319 (yellow dots) are rarer (Fig. 8a), and located only in the northern and eastern sectors of central atolls  
320 in the Tuamotu (Fig. 8d), and Gambier (Fig. 8e). Overall, the most external parts of the study region  
321 (i.e. west, south-east and north-east) are characterized by regimes occurring all around the atolls  
322 (S1, S2 and S3 respectively), which can probably be explained by a weak protection from the other  
323 atolls and small sizes (Fig. 8abd), however, in the central part of the study area (i.e. around  
324 Tuamotu), there is a clear difference between rim sections exposed to the south-west (S2) and north-  
325 east (S3 and S4).

326 Table 5 provides an average description of these five regimes. S1 and S2 have close  
327 average characteristics (relatively high  $H_s$  and  $T_p$  and a south-southwestern orientation), however  
328 S1 has slightly lower  $H_s$  and  $T_p$  than S2 and a more southerly orientation. S3 and S4 shows very  
329 different characteristics than the other regimes; they are characterized by the lowest values of  $H_s$   
330 and  $T_p$  and a north-eastern orientation. Finally, S5, which is present only at a few locations, is  
331 characterized by intermediate values of  $H_s$  and  $T_p$  and a south-east orientation.

332 These differences can be related to the spatial patterns of regional wave regimes, S1 being  
333 closely associated with R3 and S2 with R1. The shadowing effect in the central Tuamotu explains  
334 the low values of  $H_s$  and  $T_p$  and the north-eastern orientation of S3 and S4. S5, being present in  
335 eastern rims and characterized by an average south-eastern peak direction seems more associated  
336 with trade winds and therefore R2.

## 337 **4. Discussion**

338 Water renewal and quality are essential factors of the pearl farming production. These  
339 parameters are function of the lagoon circulation, itself controlled by environmental variables. In  
340 addition to tide, waves and surface winds conditions are major drivers of the lagoon circulation.  
341 While a better characterization of the South Pacific wind conditions is presented in Dutheil et al.  
342 (2020), the present study aims at better describing the wave conditions for the atolls of this region,  
343 specifically including pearl farming atolls. To describe the wave climate for the whole SCP region,  
344 as well as for atolls and for their rim sections, we used a WW3 simulation over the 2000-2017  
345 period, with a nesting strategy to increase the horizontal resolution up to  $0.05^\circ$  around atolls, and  
346 then performed a statistical clustering of wave conditions at different scales (region, atoll, rim  
347 sections). Unlike winds which have a regional pattern not particularly affected by low-lying atoll  
348 orographic effects (Dutheil et al. 2020), waves are strongly modified when crossing the  
349 archipelagos to the point that each different atoll rim section can be exposed to specific wave  
350 conditions.

351 The comparison between the simulated and observed  $H_s$  only shows a slight  
352 underestimation in our study region ( $\sim 0.1\text{m}$ ), validating the relevance of our model setup for this  
353 study. We can nevertheless discuss the likely reasons for this underestimation. Tuamotu is  
354 composed of tens of atolls including several with a size smaller than  $0.05^\circ$  (the resolution of our  
355 finer grid). The inter-atoll distance can also be of few kilometers. These different parameters (size  
356 and distance) results in a complex topography that is not accurately captured by the interpolated  
357 bathymetry on our model grid, thus modifying the interactions (reflection, dissipation, refraction)  
358 between waves and topography. In addition, a sub-grid scale obstruction parameterization is used to  
359 represent wave dissipation by sub-grid scale atolls or islands. In the WW3 model, this  
360 parameterization is only controlled by the fraction of the sub-grid scale object compared to the cell  
361 size in the x and y directions. In addition, incident swells in the SCP are mainly SW, NW, or SSE,  
362 that is “diagonal” to the model grid cells. This might induce a lower performance of the obstruction  
363 parameterization, which is computed on the x and y sections of the grid cells. Another obstruction  
364 parameterization has been recently developed (Mentaschi et al., 2018) to circumvent this issue, but  
365 has not yet been tested in the present framework. Enhanced characterization of the obstructing  
366 factor deserves future investigation.

367 To characterize the wave conditions at the regional scale, we performed a k-means  
368 clustering on 3 variables. This clustering suggested 3 regional wave regimes that can be  
369 characterized notably by their directions, respectively south-westerly (R1), south-easterly (R2) and  
370 north-westerly (R3). These 3 regimes appear to have different wave origins with remote mid-

371 latitude storm waves for R1 and R3, and a more local trade wind origin for R2. Despite the  
372 simplicity of our method to detect wave origins, there is a very good agreement with the peak  
373 direction in identified wave regimes and the detected wave origins. The only difference is in R2,  
374 which has a peak direction of 150°N in the eastern part of the domain, whereas the wave origin  
375 method points towards a 100°N origin. This difference can be explained by the clustering method,  
376 which was performed on 3 variables of equal weight and not on direction only contrary to the wave  
377 origin method. Thus, it is likely that R2 was defined by the clustering method as a regime with a  
378 short period and a low Hs, but with several wave directions including trade wind waves. This  
379 processing also explains the differences in occurrence frequency. Indeed, the wave origin method  
380 indicates a frequency of occurrence of less than 10% for waves coming from the east (Fig. 5a),  
381 whereas the frequency of occurrence of R2 is 44% (Table 2) because it probably also includes  
382 waves of other origins such as waves from the south-west and generated near the grid domain.

383         The results shown in Figures 6 to 8 provide new views of the different wave forcing that  
384 atolls, even geographically close, can experience. This has consequences to understand the unique  
385 behaviour of several atoll lagoons. For instance, it is known that several atolls have been more  
386 exposed to mortality events and algal blooms (Andréfouët et al., 2015). The knowledge of exposure  
387 to swell is not enough to explain alone mortality event occurrences, and it is necessary to also  
388 account for, at least, the rim geomorphology and the actual transfer of water from the ocean to the  
389 lagoon, but swell regimes are part of the lagoon vulnerability equation, and thus part of the pearl  
390 farming sustainability equation too. Figure 8 can be understood as a map of forcing potential  
391 induced by the mean incident wave conditions for each rim section. This part of the equation has  
392 now been clarified here.

393         The main goal of this study was to characterize the wave conditions as they are one of the  
394 major parameters controlling the lagoon circulation and thus the water quality of atolls. However,  
395 our simulation is not fine enough to compute wave transformation when approaching and entering  
396 the atoll lagoon. A transfer function evaluating how waves are transmitted into the lagoon is  
397 computed in Aucan et al. (in prep.) based on in-situ measurements. Combined with wave model  
398 results as presented here, this can be used to compute a regime of cross-reef flow to be used in  
399 hydrodynamic models of atoll lagoons (Dumas et al., 2012, Le Gendre et al, in prep.) to infer water  
400 renewal regimes.

401         The knowledge of the wave regime for each different rim section of the 83 atolls will also  
402 help understanding if atoll rim types, as for instance described for 16 Tuamotu atolls and their 117  
403 rim sections in Andréfouët et al. (2001b), can be explained by present time wave conditions. A 9-

404 class typology of rims was computed using the surface areas of vegetation, emerged area without  
405 vegetation (carbonate conglomerate), intertidal and submerged reef flat (Andréfouët et al., 2001b).  
406 Several of the rim types were related to exposure, and the role of wave forcing in explaining the  
407 typology and the distribution of the 4 types of cover was discussed by Andréfouët et al. (2001b) but  
408 not demonstrated. With the wave data presented here, this can be now explored quantitatively, with  
409 a broader geographic scope extended to 83 atolls. Furthermore, the atoll rims dominated by  
410 emerged areas without vegetation were thought to be related to tropical cyclone occurrences in the  
411 past decades (De Scally, 2008; Laurent and Varney, 2014). Waves generated by the tropical cyclones  
412 are included in our simulation thanks to a dedicated blended forcing , future studies may thus refine  
413 a typology of atoll rims and atolls using wave and rim geomorphology data.

414 Finally, we did not evaluate the impact of global warming here, but it is clear that it is an  
415 important question for atoll ecosystems. To correctly and fully evaluate the impacts of future wave  
416 conditions in a global warming context, projections of surface winds and sea level rise are  
417 necessary. Reliable projections of surface winds are available for the region from Dutheil et al.  
418 (2020), whereas projections of sea level rise are still very uncertain in Earth system models with a  
419 spread ranging between 0.3 and 1m (Stocker et al., 2014). How the atoll geomorphology will be  
420 modified with by sea level rise in the future, as well as future large-scale wave conditions remain  
421 highly uncertain (McLean and Kench, 2015).

422 To conclude, this study provides new insights on the wave conditions at atoll scale in the  
423 south Central Pacific that could be essential for assessing the potential of pearl farming atolls, and  
424 as a first step towards the construction of an atoll typology based on location, geomorphology and  
425 wave conditions. The methodology presented here is a powerful framework for characterizing wave  
426 regimes at the atoll scale, and could finally be extended to other atolls, archipelagos and basins from  
427 the Indo-Pacific, or the Caribbean Sea.

428

## 429 **Acknowledgements**

430 This study was funded by the ANR-16-CE32-0004 MANA (Management of Atolls) project. The  
431 authors acknowledge the Pôle de Calcul et de Données Marines (PCDM) for providing  
432 DATARMOR storage and computational resources (<http://www.ifremer.fr/pcdm>). The manuscript  
433 benefited from the comments provided by two reviewers.

434 **References**

- 435 Andréfouët, S., and Adjeroud, M. (2019). French Polynesia. In *World Seas: An Environmental*  
436 *Evaluation*, (Elsevier), pp. 827–854.
- 437 Andréfouët, S., Pagès, J., and Tartinville, B. (2001a). Water renewal time for classification of atoll  
438 lagoons in the Tuamotu Archipelago (French Polynesia). *Coral Reefs* 20, 399–408.
- 439 Andréfouët, S., Claereboudt, M., Matsakis, P., Pagès, J., and Dufour, P. (2001b). Typology of atoll  
440 rims in Tuamotu Archipelago (French Polynesia) at landscape scale using SPOT HRV images. *Int.*  
441 *J. Remote Sens.* 22, 987–1004.
- 442 Andréfouët, S., Ouillon, S., Brinkman, R., Falter, J., Douillet, P., Wolk, F., Smith, R., Garen, P.,  
443 Martinez, E., Laurent, V., et al. (2006). Review of solutions for 3D hydrodynamic modeling applied  
444 to aquaculture in South Pacific atoll lagoons. *Mar. Pollut. Bull.* 52, 1138–1155.
- 445 Andréfouët, S., Ardhuin, F., Queffelec, P., and Le Gendre, R. (2012). Island shadow effects and  
446 the wave climate of the Western Tuamotu Archipelago (French Polynesia) inferred from altimetry  
447 and numerical model data. *Mar. Pollut. Bull.* 65, 415–424.
- 448 Andréfouët, S., Dutheil, C., Menkes, C.E., Bador, M., and Lengaigne, M. (2015). Mass mortality  
449 events in atoll lagoons: environmental control and increased future vulnerability. *Glob. Change*  
450 *Biol.* 21, 195–205.
- 451 Ardhuin, F., Rogers, E., Babanin, A.V., Filipot, J.-F., Magne, R., Roland, A., van der Westhuysen,  
452 A., Queffelec, P., Lefevre, J.-M., Aouf, L., et al. (2010). Semiempirical Dissipation Source  
453 Functions for Ocean Waves. Part I: Definition, Calibration, and Validation. *J. Phys. Oceanogr.* 40,  
454 1917–1941.
- 455 Ardhuin, F., Rawat, A., & Aucan, J. (2014). A numerical model for free infragravity waves:  
456 Definition and validation at regional and global scales. *Ocean Modelling*, 77, 20-32.
- 457 Atkinson, M., Smith, S.V., and Stroup, E.D. (1981). Circulation in Enewetak Atoll lagoon. *Limnol.*  
458 *Oceanogr.* 26, 1074–1083.
- 459 Caldwell, P.C., and Aucan, J.P. (2007). An Empirical Method for Estimating Surf Heights from  
460 Deepwater Significant Wave Heights and Peak Periods in Coastal Zones with Narrow Shelves,  
461 Steep Bottom Slopes, and High Refraction. *J. Coast. Res.* 23, 1237.
- 462 Callaghan, D.P., Nielsen, P., Cartwright, N., Gourlay, M.R., and Baldock, T.E. (2006). Atoll lagoon  
463 flushing forced by waves. *Coast. Eng.* 53, 691–704.



464 Charrad, M., Ghazzali, N., Boiteau, V., and Niknafs, A. (2014). NbClust: An R Package for  
465 Determining the Relevant Number of Clusters in a Data Set. *J. Stat. Softw.* 61.

466 Chawla, A., and Tolman, H.L. (2008). Obstruction grids for spectral wave models. *Ocean Model.*  
467 22, 12–25.

468 Chawla, A., Spindler, D.M., and Tolman, H.L. (2013). Validation of a thirty year wave hindcast  
469 using the Climate Forecast System Reanalysis winds. *Ocean Model.* 70, 189–206.

470 De Scally, F.A. (2008). Historical Tropical Cyclone Activity and Impacts in the Cook Islands. *Pac.*  
471 *Sci.* 62, 443–459.

472 Delpy, M.T., Ardhuin, F., Collard, F., and Chapron, B. (2010). Space-time structure of long ocean  
473 swell fields. *J. Geophys. Res. Oceans* 115.

474 Dodet, G., Piolle, J.-F., Quilfen, Y., Abdalla, S., Accensi, M., Ardhuin, F., Ash, E., Bidlot, J.-R.,  
475 Gommenginger, C., Marechal, G., et al. (2020). The Sea State CCI dataset v1: towards a Sea State  
476 Climate Data Record based on satellite observations. *Earth Syst. Sci. Data Discuss.* 1–28.

477 Dumas, F., Le Gendre, R., Thomas, Y., and Andréfouët, S. (2012). Tidal flushing and wind driven  
478 circulation of Ahe atoll lagoon (Tuamotu Archipelago, French Polynesia) from in situ observations  
479 and numerical modelling. *Mar. Pollut. Bull.* 65, 425–440.

480 Dutheil, C., Andréfouët, S., Jullien, S., Le Gendre, R., Aucan, J., Menkes, C., 2020.  
481 Characterization of south central Pacific Ocean wind regimes in present and future climate for pearl  
482 farming application. *Marine Pollution Bulletin* 160, 111584.  
483 <https://doi.org/10.1016/j.marpolbul.2020.111584>

484 Diday E. (1971). Une nouvelle méthode en classification automatique et reconnaissance des formes  
485 la méthode des nuées dynamiques. *Rev. Stat. Appliquée* 19–33.

486 Hoeke, R.K., McInnes, K.L., Kruger, J.C., McNaught, R.J., Hunter, J.R., and Smithers, S.G. (2013).  
487 Widespread inundation of Pacific islands triggered by distant-source wind-waves. *Glob. Planet.*  
488 *Change* 108, 128–138.

489 Jolliffe, I. (2011). Principal Component Analysis. In *International Encyclopedia of Statistical*  
490 *Science*, M. Lovric, ed. (Berlin, Heidelberg: Springer Berlin Heidelberg), pp. 1094–1096.

491 Kraines, S.B., Suzuki, A., Yanagi, T., Isobe, M., Guo, X., and Komiyama, H. (1999). Rapid water  
492 exchange between the lagoon and the open ocean at Majuro Atoll due to wind, waves, and tide. *J.*  
493 *Geophys. Res. Oceans* 104, 15635–15653.

494 Laurent, V., and Varney, P. (2014). Historique des cyclones de Polynésie française: de 1831 à 2010  
495 (Météo France, Direction interrégionale de la Polynésie française).

496 Lecacheux, S., Pedreros, R., Le Cozannet, G., Thiébot, J., De La Torre, Y., and Bulteau, T. (2012). A  
497 method to characterize the different extreme waves for islands exposed to various wave regimes: a  
498 case study devoted to Reunion Island. *Nat. Hazards Earth Syst. Sci.* 12, 2425–2437.

499 McLean, R., and Kench, P. (2015). Destruction or persistence of coral atoll islands in the face of  
500 20th and 21st century sea-level rise? *Wiley Interdiscip. Rev. Clim. Change* 6, 445–463.

501 Mentaschi, L., Kakoulaki, G., Vousdoukas, M., Voukouvalas, E., Feyen, L., and Besio, G. (2018).  
502 Parameterizing unresolved obstacles with source terms in wave modeling: A real-world application.  
503 *Ocean Model.* 126, 77–84.

504 Piollé, J.-F., Dodet, G., and Quilfen, Y. (2020). ESA Sea State Climate Change Initiative  
505 (Sea\_State\_cci): Global remote sensing multi-mission along-track significant wave height, L2P  
506 product, version 1.1 (Centre for Environmental Data Analysis (CEDA)).

507 Quilfen, Y., and Chapron, B. (2019). Ocean Surface Wave-Current Signatures From Satellite  
508 Altimeter Measurements. *Geophys. Res. Lett.* 46, 253–261.

509 Rascle, N., and Ardhuin, F. (2013). A global wave parameter database for geophysical applications.  
510 Part 2: Model validation with improved source term parameterization. *Ocean Model.* 70, 174–188.

511 Rodier, M., Longo, S., Henry, K., Ung, A., Lo-Yat, A., Darius, H., Viallon, J., Beker, B., Delesalle,  
512 B., and Chinain, M. (2019). Diversity and toxic potential of algal bloom-forming species from  
513 Takaroa lagoon (Tuamotu, French Polynesia): a field and mesocosm study. *Aquat. Microb. Ecol.* 83,  
514 15–34.

515 Stocker, T., Alexander, L., Allen, M., Independent Police Complaints Commission, IPCC, and  
516 Working Group Science (2014). Climate change 2013 the physical science basis ; Working Group I  
517 contribution to the fifth assessment report of the Intergovernmental Panel on Climate Change  
518 (Geneva: WMO, IPCC).

519 Tartinville, B., and Rancher, J. (2000). Wave-induced flow over Mururoa atoll reef. *J. Coast. Res.*  
520 776–781.

521 Tartinville, B., Deleersnijder, E., and Rancher, J. (1997). The water residence time in the Mururoa  
522 atoll lagoon: sensitivity analysis of a three-dimensional model. *Coral Reefs* 16, 193–203.

523 Tolman, H.L. (2003). Treatment of unresolved islands and ice in wind wave models. *Ocean Model.*  
524 5, 219–231.

525 Tolman, H.L. (2009). User manual and system documentation of WAVEWATCH III TM version  
526 3.14. 220.

527 Tolman, H.L., Balasubramaniyan, B., Burroughs, L.D., Chalikov, D.V., Chao, Y.Y., Chen, H.S., and  
528 Gerald, V.M. (2002). Development and implementation of wind-generated ocean surface wave  
529 Modelsat NCEP. *Weather Forecast.* 17, 311–333.

530 Vincent, E.M., Lengaigne, M., Vialard, J., Madec, G., Jourdain, N.C., and Masson, S. (2012).  
531 Assessing the oceanic control on the amplitude of sea surface cooling induced by tropical cyclones:  
532 OCEANIC CONTROL OF TC-INDUCED COOLING. *J. Geophys. Res. Oceans* 117, n/a-n/a.

533 Woodroffe, C.D, Biribo, N., 2011. Atolls. In *Encyclopedia of Modern Coral Reefs, Structure, Form*  
534 *and Process*, ed. D. Hopley. pp. 51–71. Dordrecht, Netherlands: Springer Science+Business Media  
535 BV.

536 Young, I.R. (1999). Seasonal variability of the global ocean wind and wave climate. *Int. J. Climatol.*  
537 19, 931–950.

538

539

540 **Figure 1:** Global mean of significant wave height (in m) simulated over 2000-2017 period. (a)  
541  $0.05^\circ$  nested domain (blue box in b, c) in which the wave regimes are computed. (b) global  $0.5^\circ$   
542 domain, (c)  $0.25^\circ$  nested domain (black box in b).

543

544 **Figure 2:** Difference of significant wave height (in m) between the WW3 simulation and the  
545 altimetry measures (from CCI sea state satellite dataset) over the different domains of simulation  
546 with different horizontal resolutions a)  $0.5^\circ$ , b)  $0.25^\circ$  and c)  $0.05^\circ$ . The comparison is based on the  
547 collocation between the altimetry measurements and the data modeled on a  $0.5^\circ$  grid. Note the  
548 color-scale is refined for panel c.

549

550 **Figure 3:** Composite maps showing the temporal average of the three main regional wave regimes  
551 over the period 2000-2017. These regimes are computed on  $0.25^\circ$  grid and on [ $130^\circ\text{W}$ – $165^\circ\text{W}$  ;  
552  $9^\circ\text{S}$ – $25^\circ\text{S}$ ] domain.

553

554 **Figure 4:** Monthly mean occurrence (in number of days per month) of the three main regional  
555 waves regimes.

556

557 **Figure 5:** Percentage of occurrence of waves reaching the central point of the SCP region ( $16^\circ\text{S}$ ,  
558  $142^\circ\text{W}$  within  $\pm 5^\circ$  of the great circle route azimuth), (a) year-round, (b) in December-January-  
559 February (DJF), and (c) in June-July-August (JJA).

560

561 **Figure 6:** Cluster dendrogram classifying the wave characteristics ( $H_s$ ,  $D_p$ ,  $T_p$ ) of 83 South Pacific  
562 atolls. Green (C1), red (C2), and blue (C3) colors denote the 3 first clusters. Then the second level  
563 of clusters is also identified with dashed boxes and symbols (also pictured in Fig. 7).

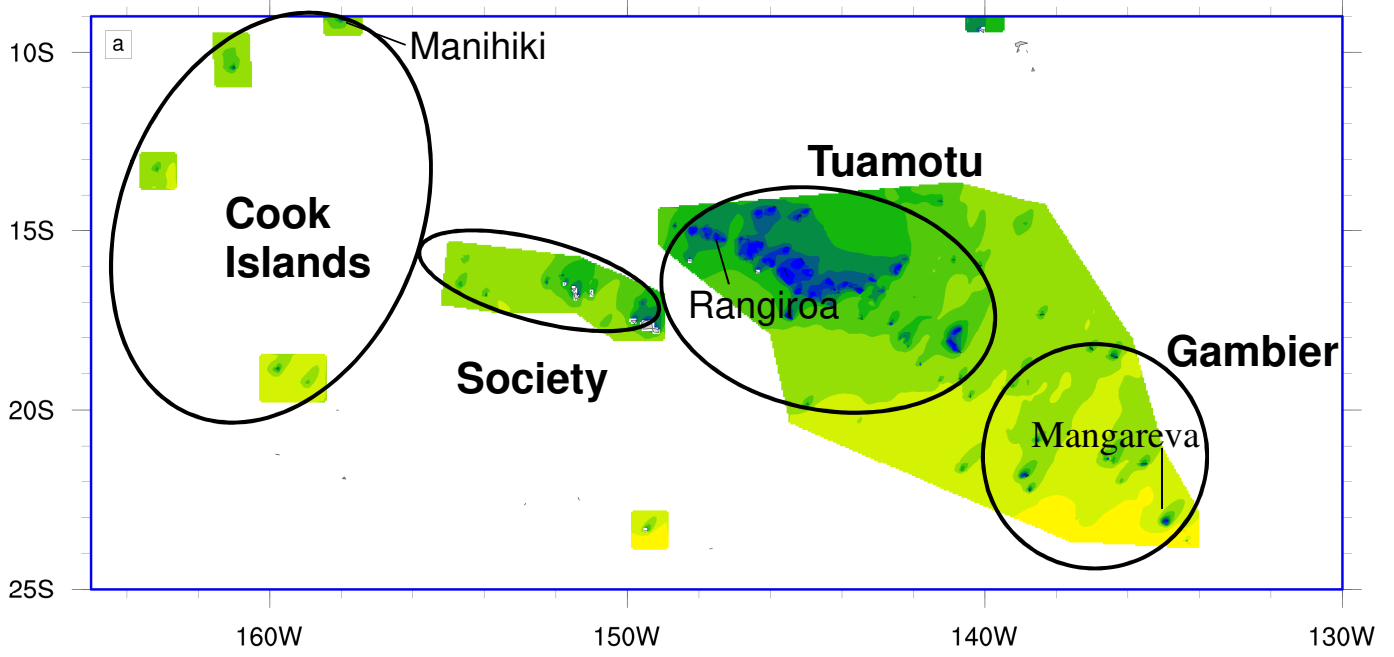
564

565 **Figure 7:** Map representing the spatial distribution in SCP of 13 wave clusters (as identified in Fig.  
566 6). As denoted in Fig. 6 colors represent the first level of clustering, and symbols the second level.  
567 Black ellipses qualitatively indicate the main archipelagoes.

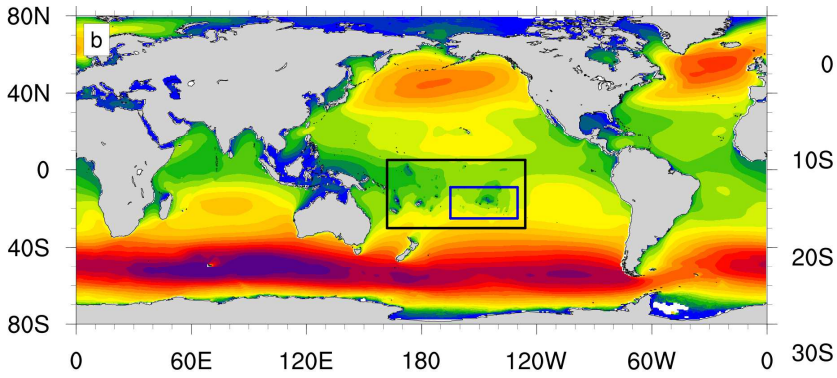
568

569 **Figure 8:** Map representing the spatial distribution of the first 5 clusters characterizing the wave  
570 conditions at the atoll rim scale. Color dots differentiate the clusters (S1: purple, S2: green, S3:  
571 blue, S4: red, S5, orange). (a) shows the whole SCP area of interest, (b-e) are zooms on (b) the  
572 Northern Cook Islands, (c) the Society, (d) the Gambier, and (e) the Tuamotu archipelagoes

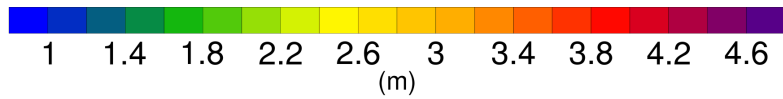
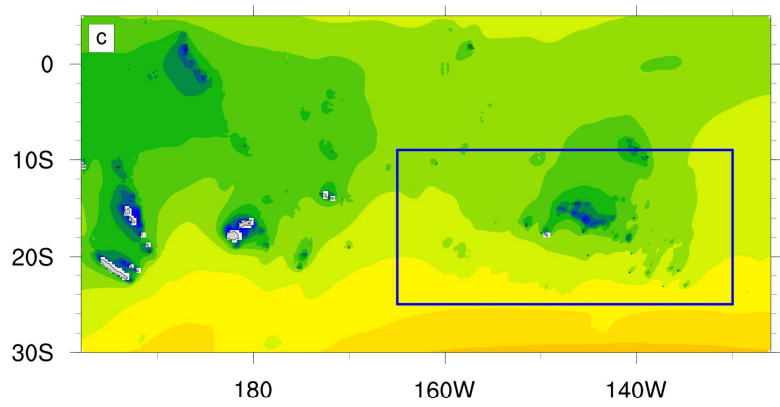
# PF-Cook domain

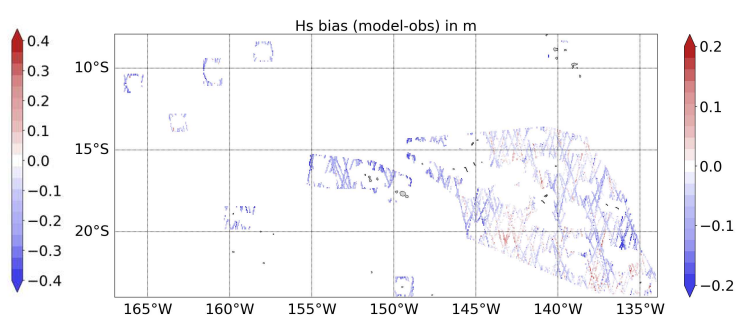
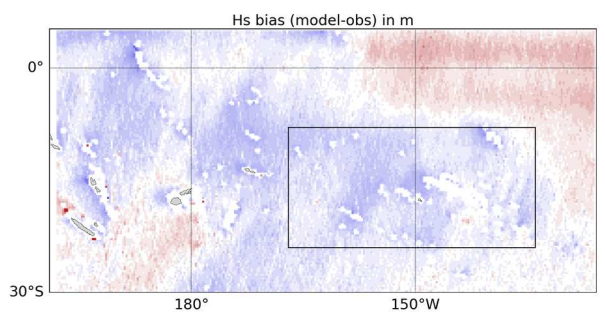
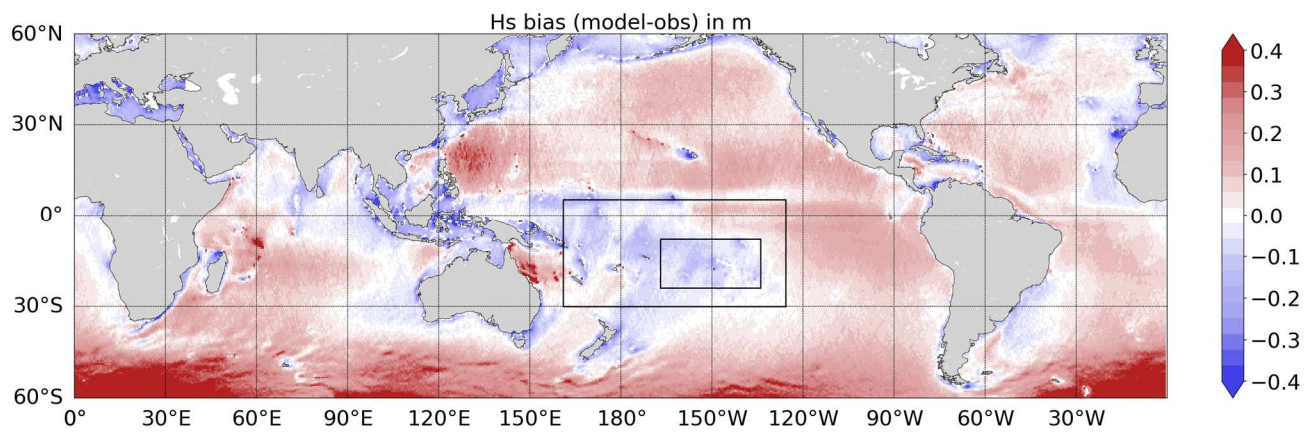


## Global domain



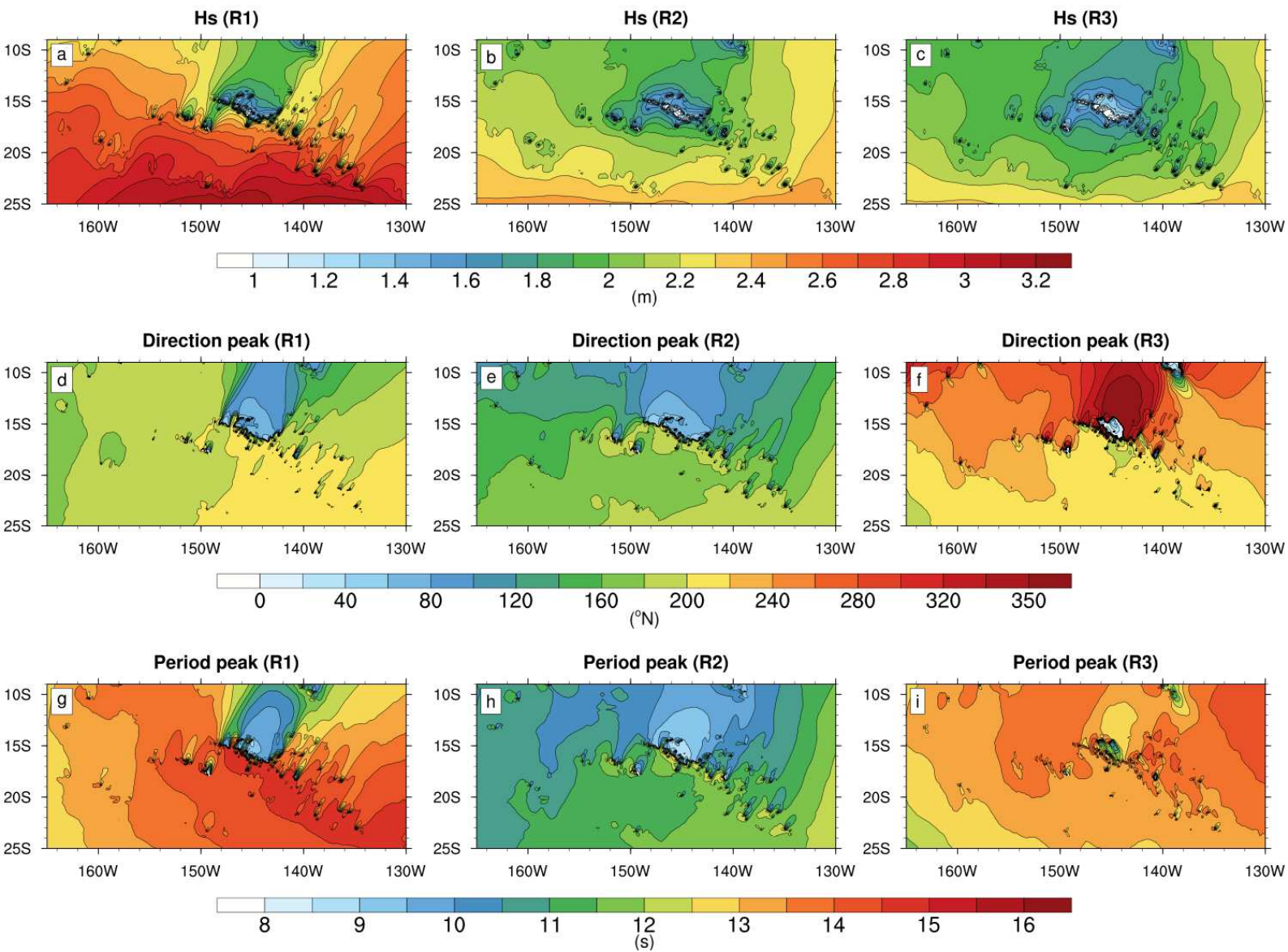
## South Pacific domain





574

Figure 2



575

Figure 3



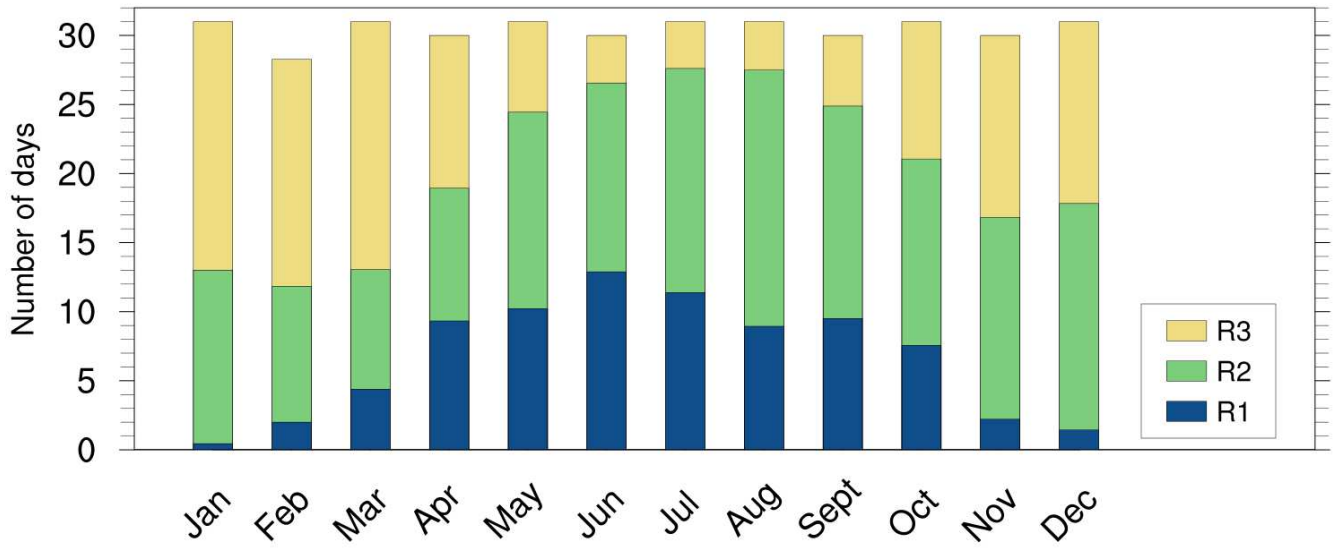
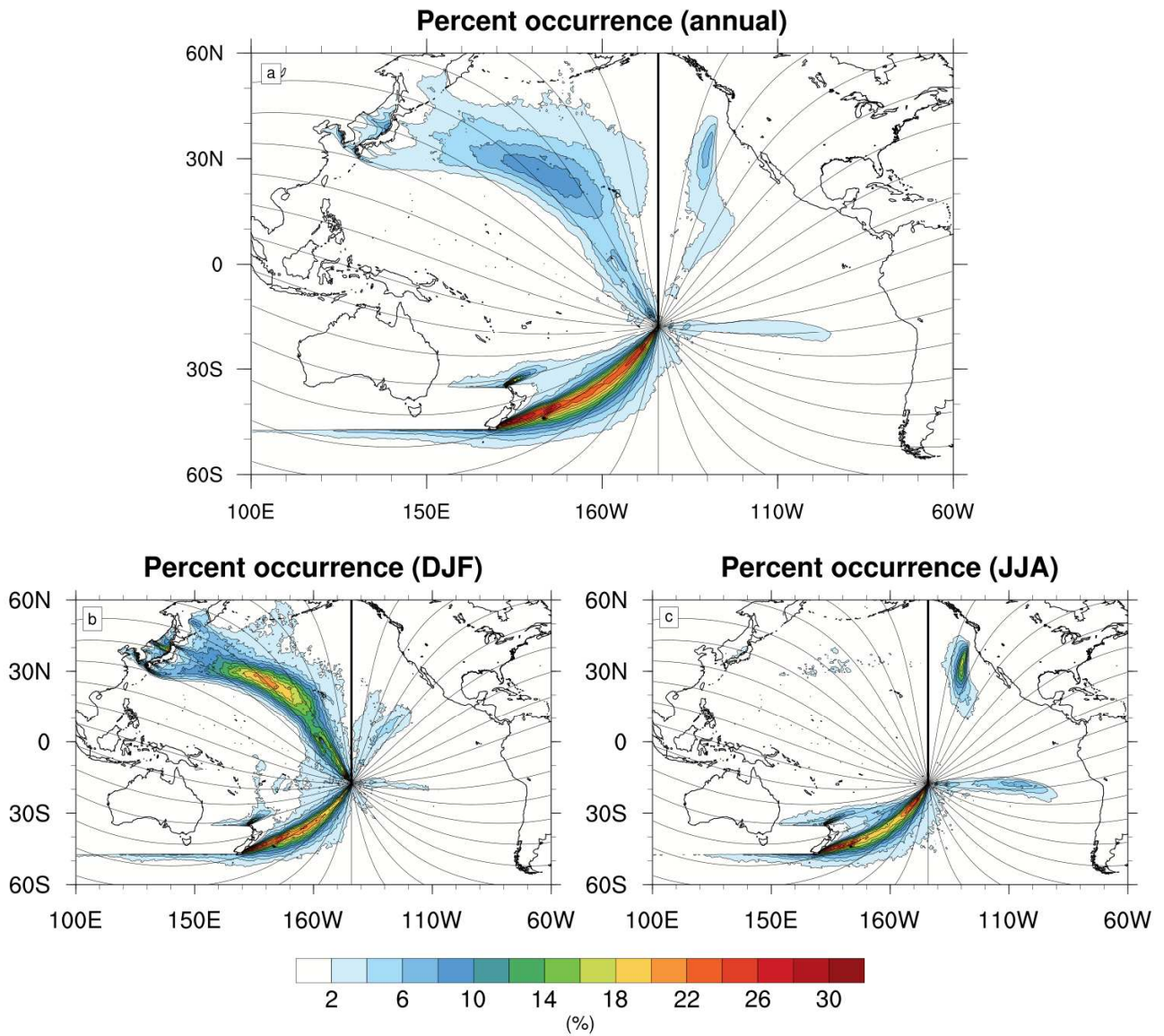


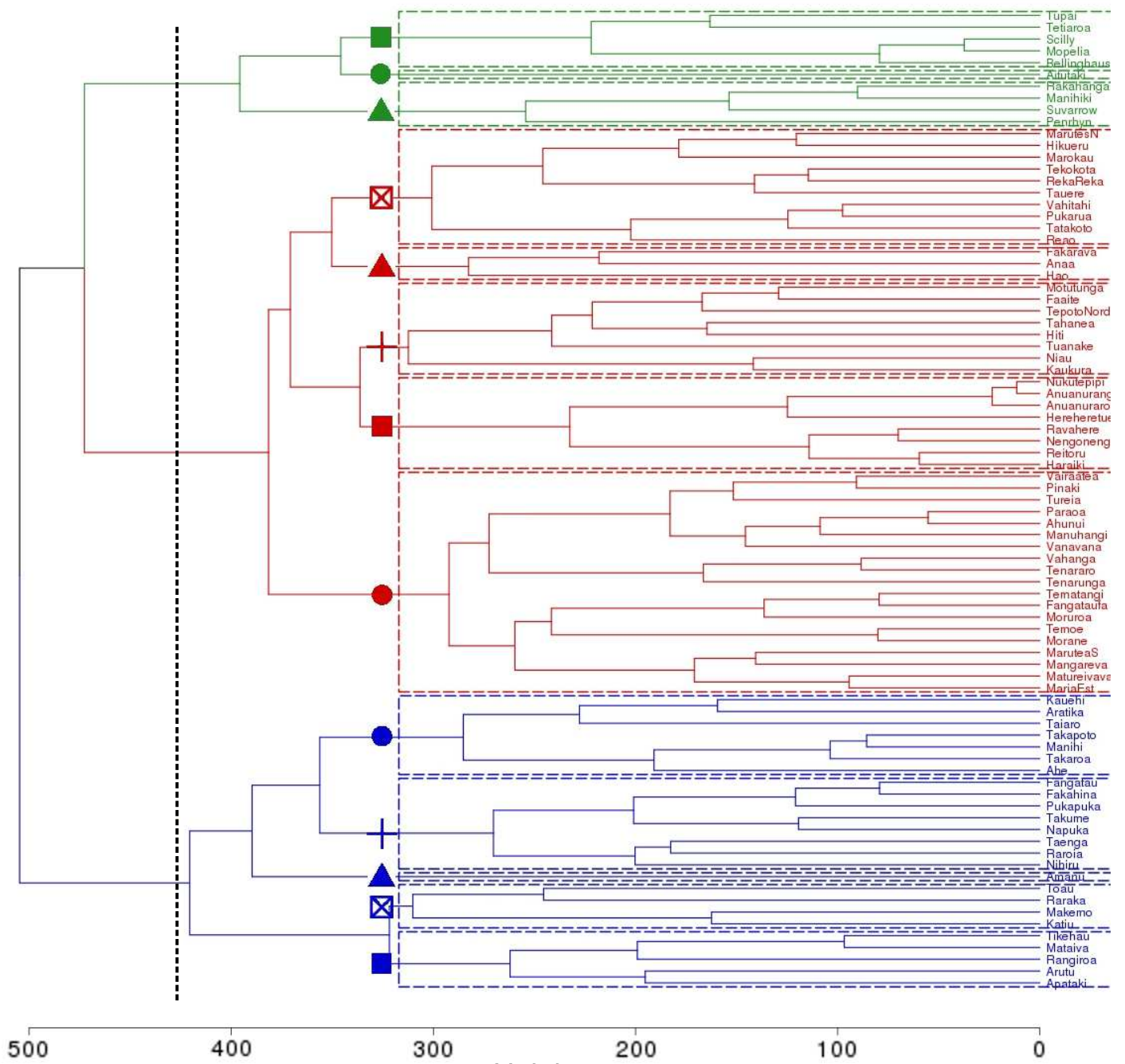
Figure 4

576



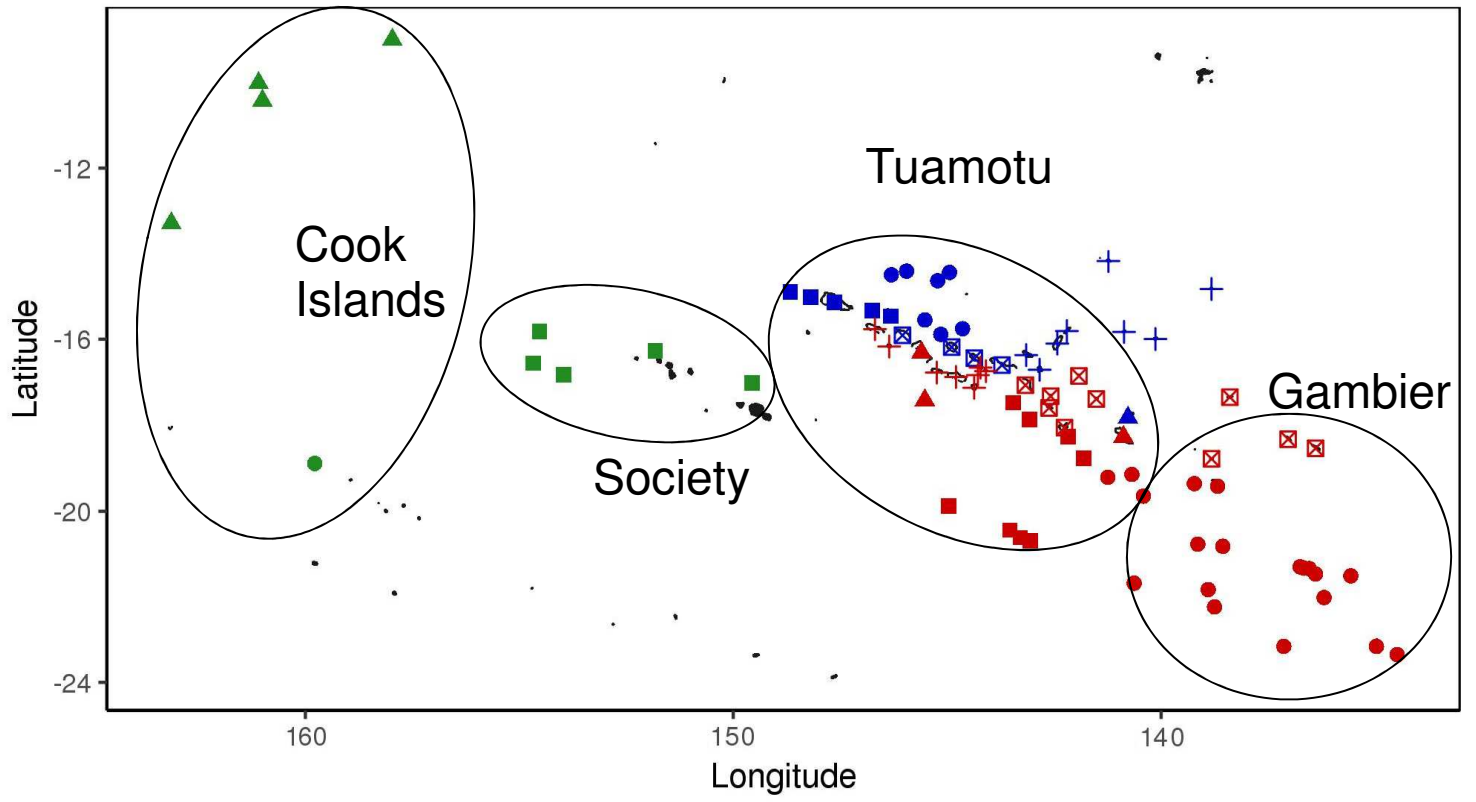


**Figure 5**



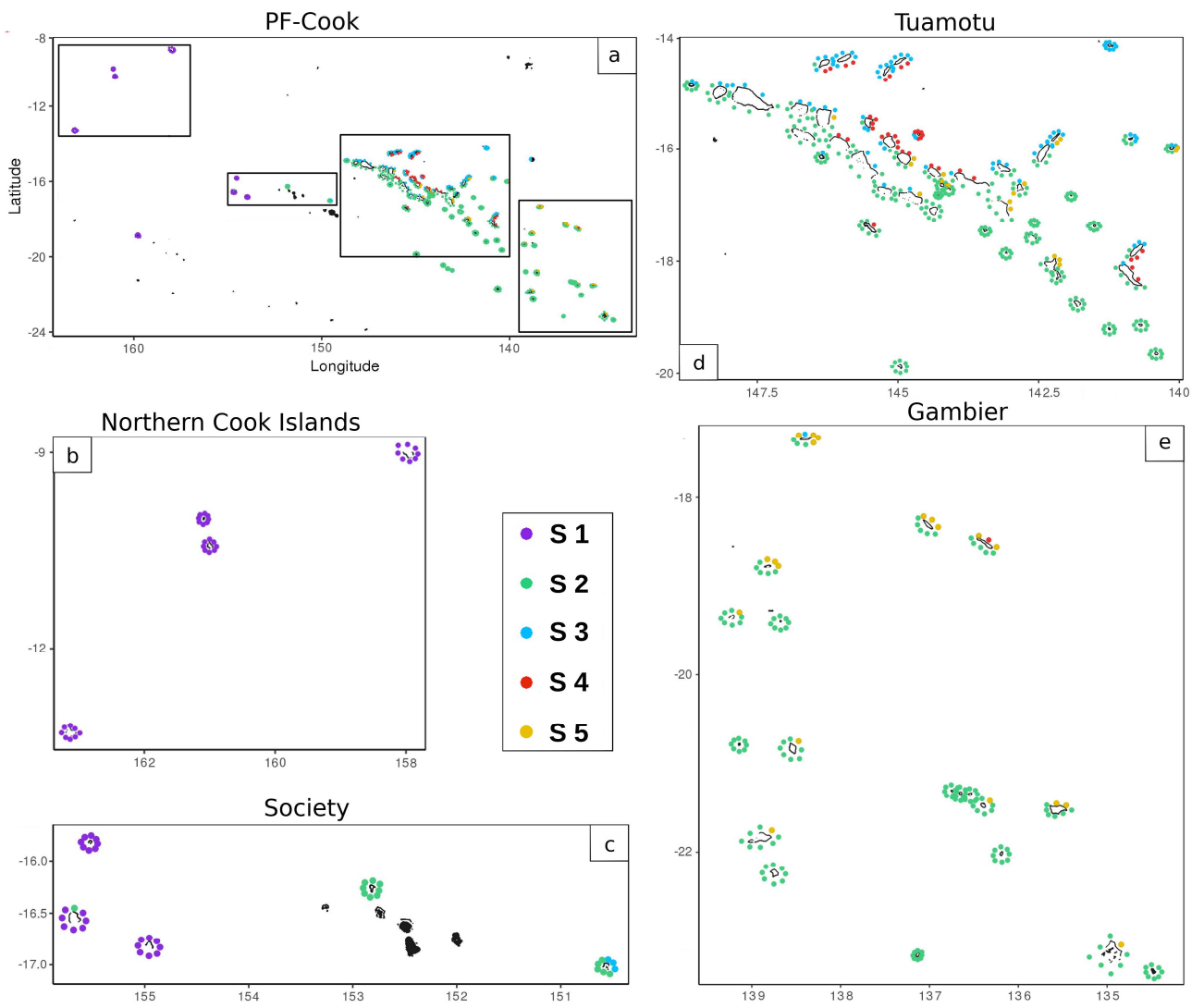
Height

Figure 6



579

Figure 7



580

Figure 8

581 **Table 1:** Numerical schemes and parameterizations used in this WW3 configuration.

WW3 switch	Description	Parameters
PR3 UQ	Ultimate Quickest third order propagation scheme (Tolman 2002)	Default values
LN1	Cavaleri and Malanotte-Rizzoli (1981) linear source term	Default values
ST4 FLX0 STAB0	Ardhuin et al. (2010) source term package	FXFM3 = 2.50 BETAMAX = 1.60000 TAUWSHELTER = 0.30000 SWELLF = 0.69000 SWELLF3 = 0.02200 SWELLF4 = 150000.0 SWELLF7 = 468000.00
NL1	Non-linear wave-wave interactions modelled using the discrete interaction approximation of Hasselmann et al. (1985)	Default values
BT4	SHOWEX bottom friction (Ardhuin et al. 2003) $\frac{\tau_b}{\rho g H}$	Default values
DB1 MLIM	Depth-induced breaking (Battjes and Janssen 1978) with a Miche-style shallow water limiter for maximum energy	Default values
REF1	Reflection at the coast	REFCOAST = 0.10 REFREQ = 1.00
IG1	Infra-gravity waves	IGMETHOD = 2 IGADDOUTP = 0 IGSOURCE = 2 IGSTERMS = 0 IGBCOVERWRITE = T IGSWELLMAX = T IGMAXFREQ = 0.0300 IGSOURCEATBP = 0 IGKDMIN = 1.1000 IGFIXEDDEPTH = 0.00 IGEMPIRICAL = 0.001250

582

583 **Table 2:** Spatial average characteristics of the three regional wave regimes.

	Frequency	Hs (in m)	Dp (in °N)	Tp (in s)
Regime 1	1446 (22%)	2.5	190.0	13.4
Regime 2	2938 (44.7%)	2.1	157.7	10.9
Regime 3	2191 (33.3%)	2.0	235.0	13.4

584

585 **Table 3:** Average characteristics of the three main wave regimes at atoll scale

	Hs (m)	Tp (s)	Dp (°N)
C1	1.82	12.34	194.07
C2	1.87	12.67	195.00
C3	1.42	11.53	113.72

586

587 **Table 4:** Average characteristics of the thirteen main wave regimes at atoll scale

	Hs (m)	Tp (s)	Dp (°N)
D1 (green squares)	1.80	12.46	203.38
D2 (green circles)	1.97	12.08	185.80
D3 (green triangles)	1.82	12.25	181.17
D4 (red square-cross)	1.81	12.49	190.58
D5 (red triangles)	1.44	12.00	184.77
D6 (red cross)	1.41	12.59	190.75
D7 (red squares)	2.05	12.80	196.20
D8 (red circles)	2.05	12.84	199.53
D9 (blue circles)	1.27	10.52	46.86
D10 (blue cross)	1.66	11.97	158.90
D11 (blue triangles)	1.32	11.00	91.19
D12 (blue square-cross)	1.25	11.72	163.17
D13 (blue squares)	1.40	12.19	198.02

588

589 **Table 5:** Average characteristics of the five first wave regimes at the scale of atoll rim sections

	Hs (m)	Tp (s)	Dp (°N)
S1	1.81	12.30	188.26
S2	1.82	12.81	198.11
S3	1.40	11.29	41.13
S4	1.28	9.44	65.30
S5	1.68	11.55	145.41

590

591